Asymptotic Analysis of n-Heptane Ignition and Cool Flames with a Temperature-Explicit Model

A. LIÑÁN

F. A. WILLIAMS

Abstract—An empirical four-step mechanism has previously been proposed for describing ignition of heptane-air mixtures. This mechanism captures the low-temperature and high-temperature ignition behavior as well as the intermediate-temperature behavior, between roughly 800 K and 1100 K, where a negative temperature dependence of the overall rate is observed. The present paper derives simplified overall rate formulas for ignition times from this four-step mechanism and uses those formulas to derive a temperature-explicit model whose simplicity facilitates analysis of more complex ignition phenomena. Methods of activation-energy asymptotics are employed for the temperature-explicit model to investigate ignition in homogeneous, adiabatic systems, ignition by compressional heating in homogeneous systems, and structures and quasisteady propagation velocities of cool flames in weakly strained mixing layers. It is shown that, in the range of negative temperature dependence, there is a plateau in the ignition time when the criterion of thermal runaway is employed. Near this plateau region, cool flames with three-zone structures can propagate at velocities that increase with increasing initial temperature. Besides providing qualitative descriptions of ignition processes for hydrocarbon-air mixtures, the results lead to quantitative predictions that can be compared with experiment.

INTRODUCTION

There is a practical interest in autoignition of hydrocarbon fuels in air, for example in connection with both Diesel-engine combustion and knock in spark-ignition engines. This has motivated experimental (Vermeer, Meyer and Oppenheim, 1972; Coats and Williams, 1979; Ciezki and Adomeit, 1993; Fieweger, Blumenthal and Adomeit, 1995; Minetti *et al.*, 1995) and computational (Coats and Williams, 1979; Westbrook, Warnatz and Pitz, 1989; Müller, Peters and Liñán, 1992; Minetti *et al.*, 1995) studies of ignition times for model hydrocarbon fuels, as well as for fuel mixtures used in applications. A favorite model fuel is n-heptane because its chemical-kinetic behavior is relatively well characterized and similar to that of other alkanes prevalent in these fuels. A four-step approximation to the detailed chemical kinetics of n-heptane ignition has been developed (Müller, Peters and Liñán, 1992) and shown to predict ignition times in good agreement with those obtained using full chemistry, between 600 K and 1500 K at 40 atm. This approximation, empirically based but with qualitative motivation from the detailed chemistry, reflects the essence of the ignition chemistry in both the low-temperature and high-temperature regimes, as well as giving good results in

between. This four-step approximation, summarized in Appendix A, is the starting point of the present investigation.

Although the four-step description is sufficiently simple that analytical methods, such as activation-energy asymptotics, can be applied to it to study ignition times in homogeneous systems (Müller, Peters and Liñán, 1992), for considering more complicated flows it can be helpful to have model chemical descriptions that are even simpler. Therefore, in the following section, it is first shown that a two-step model provides a good approximation to the four-step description, and then a one-step, temperature-explicit model is derived from this two-step model. These derivations employ asymptotic results for homogeneous, isobaric ignition times in the four-step model, given in Appendix D, which in turn were obtained from knowledge of corresponding isothermal concentration histories, presented in Appendix C, and the general mathematical formulation of Appendix B for nonhomogeneous systems. After it is derived, the temperature-explicit model is applied here to three sequentially more complicated ignition problems - first homogeneous, isobaric explosions in adiabatic systems, next ignition achieved through heating by external compression in homogeneous systems, and finally the structure and propagation of cool flames in nonhomogeneous systems. These three applications illustrate the utility of the temperature-explicit description for describing ignition phenomena over a wide range of initial temperatures.

THE TWO-STEP AND ONE-STEP CHEMICAL MODELS

In the four-step model presented in Appendix A, the first two steps, Eqs. (A1) and (A2), describe the high-temperature path and the next two, Eqs. (A3) and (A4) the low-temperature path. The studies in Appendices C and D demonstrate that, whenever the high-temperature intermediate I is important, it obeys a steady-state approximation quite well. It therefore follows that Eq. (C12) can be used for the mole fraction of this intermediate throughout all ignition analyses, any initial period in which this equation is invalid is being negligibly short. The resulting algebraic equation removes I from the system, effectively combining Eqs. (A1) and (A2), and thereby yields a three-step description, in which the production rates W_F, W_J and W_O of Eqs. (B13), (B15) and (B16), for example, may be taken as the independent rates.

Unlike I, the low-temperature intermediate J does not achieve a steady state over the ignition conditions of interest, except at the higher temperatures, as seen in Appendices C and D. It is therefore not possible to obtain a reasonable two-step model simply by putting J into steady state. Closer attention must therefore be paid to the detailed characteristics of ignition in deriving a two-step approximation.

The mechanism in Eqs. (A1)–(A4) involves only straight chains and therefore is not subject to branched-chain explosions. It follows that thermal explosion theory is the appropriate way to address ignition problems for this mechanism. In the theory of thermal explosions, reactant consumption can be neglected in the first approximation, so that rates such as W_F and W_O become not directly relevant but enter only to the extent that they affect the heat-release rate W_T. Therefore, it is relevant to focus on energy conservation, Eq. (B10), in seeking further possible simplifications.

With the steady state for I, Eq. (C12), the expression for W_T given in Eq. (B18) can be simplified if T_3 is neglected in comparison with T_4. According to Eq. (A9), this is a very good approximation, that is, the reversible step in Eq. (A3) is very nearly energetically neutral. With this approximation, Eq. (B18) becomes

$$W_T = T_Q(k_1 X_F + k_4 n X_O X_J), \tag{1}$$

where $T_Q = 128{,}700$ K is within 1% of both T_4 and $T_1 + T_2$. Equation (1) indicates that, energetically, both the low-temperature path through k_4 and the high-temperature path through k_1 have essentially the same heat release, measured by T_Q. At high temperatures, this energy release, through steps 1 and 2, occurs at the rate of step 1, while at low temperatures it occurs through step 4, at a rate that depends on the concentration of the intermediate J, which is produced by the forward step 3, found in Appendices C and D to proceed at a rate as important as that of step 4 throughout the low-temperature range of interest.

With changes of X_F and X_O neglected, use of Eq. (1) for describing ignition in the low-temperature range still necessitates addressing the history of X_J. The reasoning leading to Eq. (D6) indicates that, over the entire range of conditions for which the model chemistry applies, the contribution of ω_4 to W_J in Eq. (B15) is negligible compared with that of ω_3 throughout the ignition period; the criterion for this to be true is $k_4 n X_O (k_{3f} n X_O X_F t_{ign}) \ll k_{3f} n X_O X_F$ in which X_J has been estimated from Eq. (D5), and use of Eq. (D6) in this inequality reduces it to $\beta_o \equiv X_{Fo} T_Q T_A / T_o^2 \gg k_4/k_{3f}$, which is violated only at very low initial temperatures. The effect of the reverse step 3b becomes important in W_J when $k_{3b}(k_{3f} n X_O X_F t_{ign}) \geqslant k_{3f} n X_O X_F$, that is $\beta_o \leqslant k_{3b}/(k_5 X_{Oo}^2)$, where use has been made of Eqs. (C10) and (D6). This last condition is achieved at about 900 K at 40 atm and at about 800 K at 4 atm, and it signals the beginning of the region of negative temperature dependence, discussed in Appendices C and D. In general, then, to span all regimes, Eq. (1) may be supplemented by

$$W_J = k_{3f} n X_O X_F - k_{3b} X_J \tag{2}$$

effectively providing a two-step description for ignition.

Equations (1) and (2), with Eq. (B9) for $j = J$ and Eq. (B10), yield a two-equation model for describing ignition processes when X_F and X_O are prescribed. This two-equation description, simpler than the original six-equation description that results from the four-step model, could be used to investigate many ignition phenomena accurately. However, to expose the character of the ignition even more simply, it is helpful to have a one-equation, temperature-explicit model. Such a model can readily be proposed from the information that has now been developed.

All the significant regimes that have been identified are captured by the model

$$W_T = T_Q(R_L + R_H),$$

where the low-temperature and high-temperature rates are, respectively,

$$R_L = B_L e^{-T_L/T}/(1 + B_I e^{-T_I/T}), \quad R_H = B_H e^{-T_H/T}. \tag{4}$$

Here

$$T_H = T_a = 21{,}650\,\mathrm{K},\ T_L \equiv aT_H = (T_a + T_c)/2 = 17{,}440\,\mathrm{K},$$
$$T_I \equiv bT_H = T_b - (T_a + T_c)/2 = 19{,}845\,\mathrm{K}, \tag{5}$$

so that $a = 0.806$ and $b = 0.917$, and

$$\left.\begin{aligned} B_H &= A_1 X_{Fo} \equiv A_H X_{Fo}, \\ B_L &= (A_{3f}A_4)^{1/2}(n_o X_{Oo})\, X_{Fo}^{1/2}\, T_o/(T_Q T_L)^{1/2} \equiv A_L(n_o X_{Oo})\, X_{Fo}^{1/2}\, T_o, \\ B_I &= [A_{3b}/(A_{3f}A_4)^{1/2}]\,(n_o X_{Oo})^{-1} X_{Fo}^{-1/2}\, T_o/(T_Q T_L)^{1/2} \equiv A_I(n_o X_{Oo})^{-1} X_{Fo}^{-1/2}\, T_o, \end{aligned}\right\} \tag{6}$$

where $A_H = 2.0 \times 10^{10}\mathrm{s}^{-1}$, $A_L = 2.6 \times 10^{11}(\mathrm{cm}^3/\mathrm{mol})\mathrm{s}^{-1}\mathrm{K}^{-1}$ and $A_I = 69\ (\mathrm{mol}/\mathrm{cm}^3)\ \mathrm{K}^{-1}$. The additive term in the denominator of R_L involving B_I accounts for the approach of species J to its steady state (defined by partial equilibrium of step 3) in the intermediate temperature range of negative temperature sensitivity. From the two-step model it is clear that this model can be derived rigorously to leading order in activation-energy asymptotics for the high-temperature and intermediate-temperature ranges but not when the contribution from the low-temperature range is significant, since in this range the two-step character cannot be removed formally. The low-temperature character is reflected in the parameters B_L and T_L, whose expressions have been selected so that the classical Frank-Kamenetskii ignition theory produces Eq.(D6) for the ignition time in this range.

Figure 1 is a schematic illustration of the temperature-explicit rate, with the high-temperature and the low-temperature ranges, as well as the intermediate range of negative temperature dependence, shown explicitly. Various parameters are indicated on the curve in Figure 1 for use in subsequent analyses.

HOMOGENEOUS, ISOBARIC EXPLOSION IN THE TEMPERATURE-EXPLICIT MODEL

The temperature-explicit model has two special temperatures, one where R_L achieves a maximum (with R_H negligible) and another, higher temperature, where $R_L + R_H$ is a minimum, as seen in Figure 1. The main interest here is in determining the homogeneous ignition behavior in the vicinity of the range of these two temperatures, since far outside that range either $W_T = T_Q B_L e^{-T_L/T}$ or $W_T = T_Q B_H e^{-T_H/T}$, and the behavior is well known. It is convenient to define crossover temperatures T_β and T_α, by

$$B_I e^{-bT_H/T_\beta} = 1, \quad (B_L/B_I)\, e^{(b-a)T_H/T_\alpha} = B_H e^{-T_H/T_\alpha}, \tag{7}$$

as illustrated in Figure 1. With these definitions, T_β is near the maximum of R_L and $T_\alpha > T_\beta$ is near the minimum of $R_L + R_H$. In the variables

$$\theta = (T_H/T_\beta^2)(T - T_\beta), \quad \tau = t(T_Q T_H/T_\beta^2)\, B_L e^{-aT_H/T_\beta}, \tag{8}$$

Eq. (B22) for $j = T$ with Eq.(3) becomes

$$d\theta/d\tau = e^{a\theta}/(1 + e^{b\theta}) + e^{-(1+b-a)\theta_s + \theta} \tag{9}$$

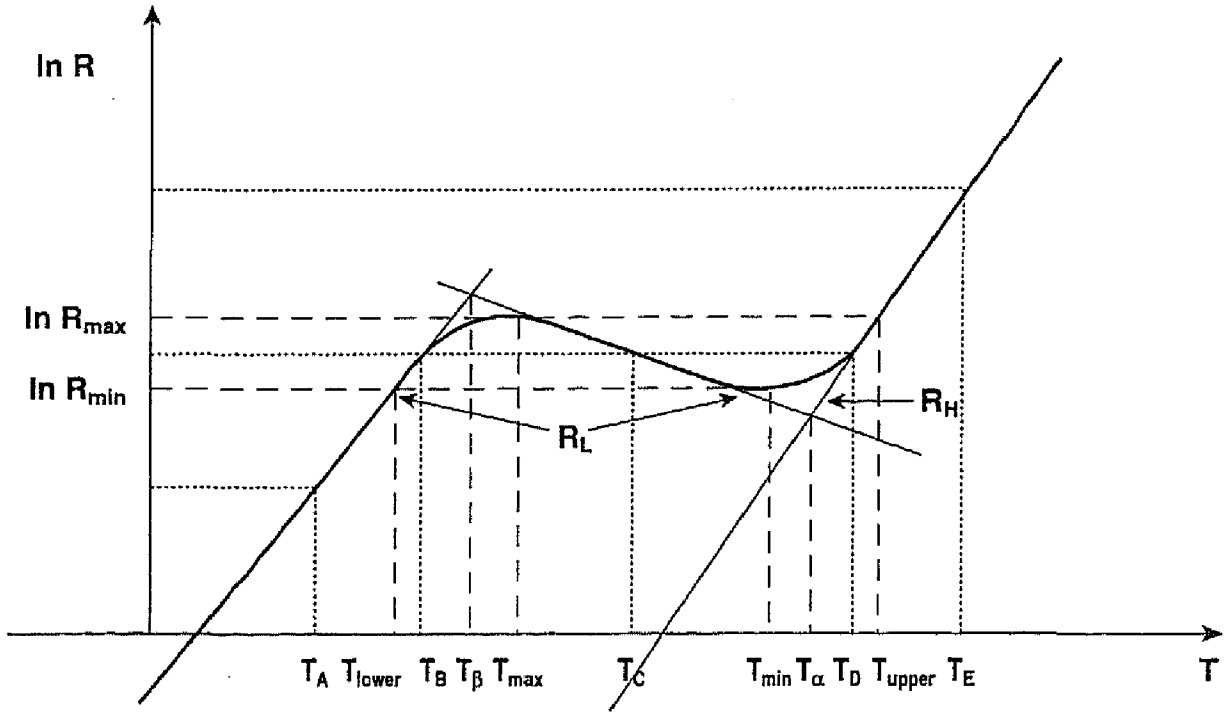

FIGURE 1 A schematic semilog graph of the temperature-explicit rate as a function of temperature, illustrating critical temperatures and rates.

to leading order in the small parameter T_β/T_H, where $\theta_\alpha \equiv (T_H/T_\beta^2)(T_\alpha - T_\beta)$. Here $(T_\alpha - T_\beta)/T_\beta$ has been considered to be small enough for θ_α to be of order unity, which is the condition that prevails in the heptane problem. The initial condition for Eq. (9) is $\theta = \theta_o$ at $\tau = 0$, where $\theta_o \equiv (T_H/T_\beta^2)(T_o - T_\beta)$.

In the ordinary theory of thermal explosion for the low-temperature regime, the right-hand side of Eq. (9) is simply $e^{a\theta}$, and the solution exhibits thermal runaway ($\theta \to \infty$) at an ignition time defined by $a\tau = 1$. Since $b > a$, the factor $1 + e^{b\theta}$ in the denominator prevents this from occurring and instead causes θ to tend to level off in a plateau range identified here as θ_p. When $-\theta \gg 1$ and $0 \ll \theta_p \ll \theta_\alpha$, there exists a first stage, $\theta_o \leqslant \theta \leqslant \theta_p$, during which the last term in Eq. (9) is negligible, and integration may be performed to give

$$\tau = (e^{-a\theta_o} - e^{-a\theta})/a + [e^{(b-a)\theta} - e^{(b-a)\theta_o}]/(b-a). \tag{10}$$

As time proceeds, $e^{(b-a)\theta}$ increases and $e^{-a\theta}$ decreases, so that $e^{(b-a)\theta_o}$ and $e^{-a\theta}$ eventually become negligible, and the plateau condition, in which

$$\tau_p = e^{-a\theta_o}/a + e^{(b-a)\theta_p}/(b-a), \tag{11}$$

is reached.

When θ becomes comparable with θ_α, a second begins in which the last term in Eq. (9) is no longer negligible, and this last term then eventually causes thermal runaway. In this second stage (as during the plateau period), $e^{b\theta} \gg 1$, so Eq. (9) simplifies to

$$d\varphi/d\tau = e^{-(b-a)\theta_\alpha}[e^{-(b-a)\varphi} + e^{\varphi}], \tag{12}$$

where $\varphi = \theta - \theta_\alpha$. Formal integration from $\varphi = \varphi_p \equiv \theta_p - \theta_\alpha$ at $\tau = \tau_p$ gives

$$\int_{\varphi_p}^{\varphi} [e^{-\varphi}/(1 + e^{-c\varphi})]d\varphi = e^{-(b-a)\theta_\alpha}(\tau - \tau_p), \tag{13}$$

where $c \equiv 1 + b - a$. Thermal runaway ($\varphi \to \infty$) occurs in Eq. (13) at an ignition time τ_i, defined by

$$\tau_i = e^{-a\theta_0}/a + e^{-(b-a)\theta_\alpha}\left\{\int_{\varphi_p}^{\infty} [e^{-\varphi}/(1 + e^{-c\varphi})]d\varphi + e^{(c-1)\varphi_p}/(c-1)\right\}, \tag{14}$$

where use has been made of Eq. (11). With $\theta_p \ll \theta_\alpha$ and θ_α sufficiently large, φ_p is large and negative, so that Eq. (14) becomes

$$\tau_i = e^{-a\theta_0}/a + e^{-(b-a)\theta_\alpha} I(c), \tag{15}$$

where the integral I has been defined as

$$I(c) \equiv \int_{-\infty}^{\infty} [e^{-\varphi}/(1 + e^{-c\varphi})]d\varphi = (\pi/c)/\sin(\pi/c). \tag{16}$$

Equation (15) exhibits two additive contributions to τ_i, the first ($e^{-a\theta_0}/a$) which would apply if thermal runaway were to occur in the low-temperature regime, and the second associated with thermal runaway in the high-temperature regime after passage through the range of negative temperature dependence. The term involving the factor $I(c)$ thus represents the time needed to traverse the intermediate range, which is dominant when $-a\theta_0 \ll (b-a)\theta_0$ while the low-temperature contribution is dominant when $-a\theta_0 \gg (b-a)\theta_\alpha$.

At higher initial temperatures, when the system initially is in the plateau range or above, $e^{b\theta} \gg 1$ always in Eq. (9), so that the approximation leading to Eq. (12) applies from the outset, and use of $\theta \equiv \theta_0$ at $\tau = 0$ then gives

$$\tau_i e^{-(b-a)\theta_\alpha} = \int_{\theta_0 - \theta_\alpha}^{\infty} [e^{-\varphi}/(1 + e^{-c\varphi})]d\varphi \equiv F(\theta_0 - \theta_\alpha, c), \tag{17}$$

a monotonically decreasing function of $\theta_0 - \theta_\alpha$ that approaches $e^{-(\theta_0 - \theta_\alpha)}$ when $\theta_0 - \theta_\alpha \gg 1$, giving $\tau_i = e^{-\theta_0} e^{c\theta_\alpha}$, identifiable from Eqs. (7) and (8) as the ordinary ignition time that would be obtained in the high-temperature regime alone. As $\theta_0 - \theta_\alpha \to -\infty$, $F(\theta_0 - \theta_\alpha, c) \to I(c)$, reproducing the result from Eq. (15) with the first term negligible. Thus, Eqs. (15) and (17) span the entire range of ignition behavior.

The general characteristics of the temperature-time histories in the homogeneous thermal explosion are illustrated schematically in Figure 2. At low temperatures, below the value of T_r of Eq (D12), from the analysis of Appendix D, or below T_{lower} of Figure 1 for the present analysis, the behavior is as predicted for ordinary thermal explosions (with B_I and B_H zero). Similarly, above the temperature T^* of Eq. (D14), for the analysis of Appendix D, or above T_{upper} of Figure 1, again there is an ordinary thermal explosion (now with B_I and B_L zero). In the intermediate range, the temperature predicted by Eq. (9) nearly levels off at a plateau value, illustrated in Figure 2, and increases only very gradually, until the temperature becomes high enough for the high-temperature chemistry to take control and cause thermal explosion. The consequent ignition times

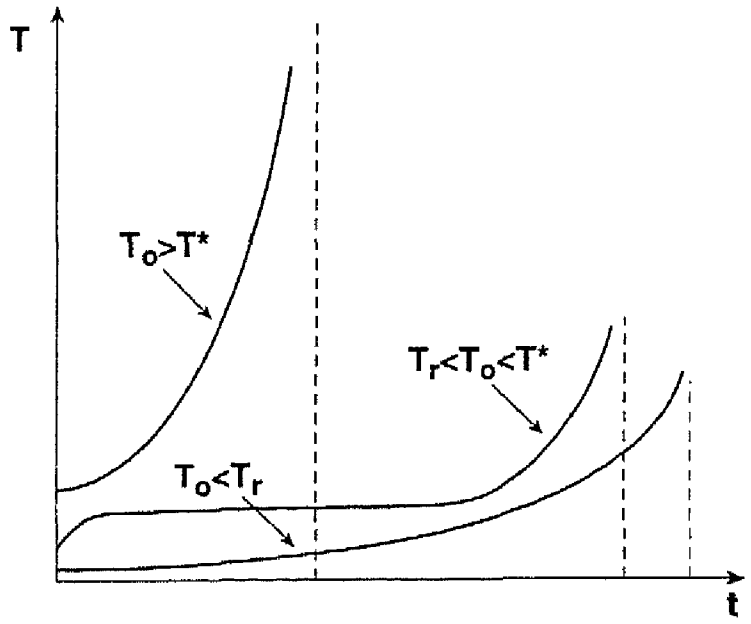

FIGURE 2 A schematic illustration of temperature-time histories during ignition in different regimes.

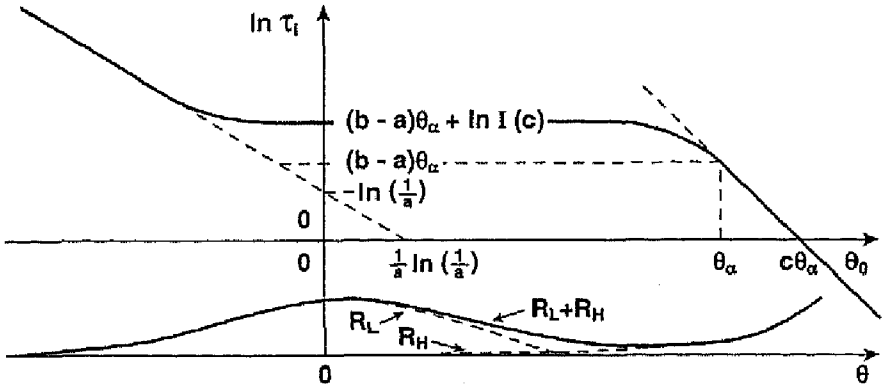

FIGURE 3 The nondimensional ignition time as a function of the nondimensional initial temperature, according to the approximation of the temperature-explicit rate.

from the present analysis are shown in Figure 3. It may be noted from Figure 3 that, when the criterion of thermal runaway is employed to define ignition, the ignition time is monotonic in temperature, exhibiting a plateau but not a dip. This occurs because thermal runaway cannot arise in the region of negative temperature dependence.

IGNITION UNDER HEATING BY EXTERNAL COMPRESSION

The effects of pressure changes on ignition for one-step, Arrhenius chemistry have been analyzed previously (Liñán and Williams, 1995). By introducing the entropy variable $T/p^{(\gamma-1)/\gamma}$, a formulation like that for isobaric ignition is recovered, with the compressional heating taken into account. A general discussion of how the results for one-step chemistry can be extended to the four-step heptane model is given in an appendix of the earlier paper (Liñán and Williams, 1995). However, no detailed analysis is presented

there. Therefore, it is of interest to show here what are implications of the temperature-explicit model for ignition produced by compressional heating in a homogeneous system.

In Eq. (B10) without the space derivatives, the pressure term can be denoted by $T_Q R$, where $R(t)$ is a prescribed rate function determined from the compressional heating rate. Use of Eq. (3) in the resulting differential equation then gives

$$dT/dt = T_Q(R_L + R_H + R), \tag{18}$$

where R_L and R_H are defined in Eq. (4). The initial condition is $T = T_o$ at $t = 0$. The effect of compressional heating may be seen most simply by taking R to be a prescribed constant.

The ignition history for this problem depends on propereties of $R_L + R_H$ that are illustrated in Figure 1. This rare achieves a maximum value, $R_{\max}$, at a temperature $T_{\max}$ determined by

$$B_I e^{-bT_H/T_{\max}} = a/(b-a), \tag{19}$$

then achieves a minimum value, $R_{\min}$, at a hiegher temperature $T_{\min}$ determined by

$$(B_H B_I/B_L) e^{-(1+b-a)T_H/T_{\min}} = a/(b-a), \tag{20}$$

as found from Eq. (4) by setting derivatives to zero. Substitution of these results into Eq. (4) gives the rate extrema as

$$R_{\max} = (B_L/b)(a/B_I)^{a/b}(b-a)^{(b-a)/b} \tag{21}$$

and

$$R_{\min} = (B_L/B_I)^{1/c} B_H^{(b-a)/c}[(b-a)^{-(b-a)/c} + (b-a)^{1/c}], \tag{22}$$

where $c = 1 + b - a$. Eq. (6) can be used to relate these parameters back to those of the original four-step model. The ignition history depends on the relationship between the external rate R and the values $R_{\max}$ and $R_{\min}$.

If $R < R_{\min}$ and T_o is sufficiently far below T_{lower}, illustrated in Figure 1, then in Eq. (18) initially $dT/dt = T_Q R$, and the compressional heating dominates until $R_L = R$, that is, $B_L e^{-T_L/T} = R$, at which time a weak ignition occurs. The temperature T_A in Figure 1 is an illustrative solution to this last equation, and the corresponding temperature history is illustrated by the lower curve in Figure 4. At these low values of R, after the temperature reaches T_A the compressional heating remains small compared with the chemical heating, and the problem becomes equivalent to that analyzed in the preceding section for $-\theta_o \gg 1$. A plateau range (not illustrated in Fig. 4) is thus encountered prior to the strong thermal runaway.

If $R_{\min} < R < R_{\max}$ and $T_o < T_{\text{lower}}$, then in Eq. (18) $R_L + R_H$ remains small compared with R until the inert temperature reaches a value of T_B, illustrated in Figure 1, at which $R_L = R$. The chemical heating then dominates and, as illustrated by the middle curve in Figure 4, causes a more rapid temperature increase, until temperature T_C is reached, at which the time the compressional heating again becomes larger than the chemical heating. The compressional heating establishes the minimum rate of temperature rise, which persists to temperature T_D, defined by $R_H = R$, at which point the high-temperature reaction becomes dominant and causes a strong ignition, illustrated at the

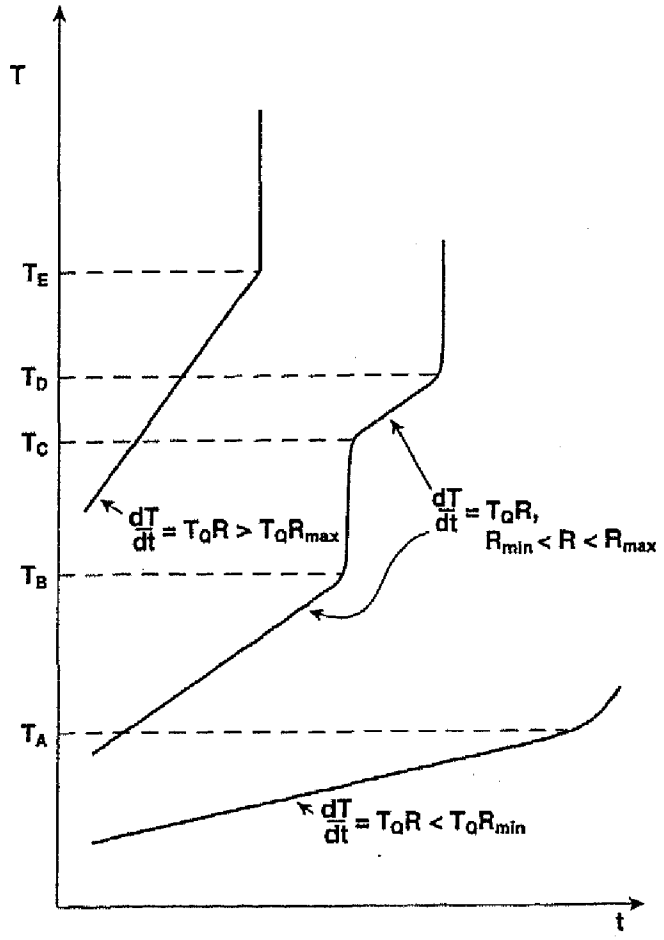

FIGURE 4 A schematic illustration of representative temperature-time histories for ignition by external compression.

upper end of the middle curve in Figure 4. The temperature-time history for compressional ignition can thus exhibit fairly complex behavior in this intermediate range of heating rate.

If $R > R_{max}$ and $T_o < T_{upper}$, then the compressional heating rate exceeds the chemical heating rates of the low-temperature and intermediate ranges, and only R_H can compete with R. In this case, the temperature increases by inert compressional heating until $R_H = R$, illustrated at temperature T_E in Figure 1, at which temperature a strong ignition occurs. The upper curve in Figure 4 illustrates this temperature-time history. Although more detailed analyses can be developed for more specifically prescribed pressure histories, the present discussion should be sufficient for indicating the full range of behaviors that can occur.

COOL FLAMES

Attention thus far has been restricted to problems exhibiting spatial homogeneity. Many problems that involve space dependences can be addressed on the basis of the formulation given in Appendix B. In unstrained mixing layers, characteristic inert diffusion times typically are long compared with ignition times, and relevant analyses

of ignition stages in such nonhomogeneous systems often can make direct use of the preceding space-independent descriptions. Imposing strain on mixing layers can reduce characteristic diffusion times substantially. For steady, strained mixing layers, ignition cannot occur if the strain rate is too large; relevant parameters here will be Damkhler numbers related to $(At_{ign})^{-1}$, for the A of Eq.(B8). At sufficiently high temperatures, analyses based on one-step activation-energy asymptotics (Liñán and Williams, 1993a) can be employed directly, but at lower temperatures, the greater complexity of the chemistry necessitates further analysis. An interesting phenomenon that can occur at these lower temperatures is transient propagation of cool flames, the final topic to be addressed in the present paper.

A great deal of information is available in the literature on cool-flame phenomena (e.g., Lewis and von Elbe, 1987). Cool flames may be generated in experiments involving adiabatic compression of hydrocarbon-air mixtures, for example, and under idealized laboratory conditions they often appear to occur homogeneously throughout the compressed system, frequently repeatedly in time. However, by use of specially designed burners (Williams, Johnson and Carhart, 1959), they can be stabilized in laboratory flow systems to study their structures (Williams and Sheinson, 1973), which then exhibit spatial dependence. The steady-state spatial structures and steady propagation velocities of cool flames are analyzed theoretically here. Except for one treatment of a different model (Nicoli, Clavin and Liñán, 1987), a two-equation model involving chain branching, no corresponding theoretical cool-flame analyses have been completed. The steady-state structures need to be known before transient cool-flame behavior can be studied properly. Beginning with the results to be derived here, future work could reasonably address questions of time-dependent cool-flame dynamics.

Consider a moderately strained mixing layer subject to moderate compressional heating. At some point in the mixing layer, in Diesel applications typically near the air side where the temperature is the highest, a weak ignition of the type described in the previous section for $R < R_{min}$ is presumed to occur. This ignition can acceleratively increase the local temperature to T_{max} of Figure 1, but thereafter the rate slows (until temperature T_{min} is reached). During this period, the fuel adjacent to the weakly ignited region may begin to be heated by conduction from the region having temperature T_{max}. This conductive heating may then result in propagation of a cool-flame type of deflagration towards the fuel side of the mixing layer. The problem to be addressed concerns the structures and propagation velocities of these cool flames that propagate from ignition spots in mixing layers. The extent of fuel consumption in these cool flames often is small, so that more than one cool flame can be generated and propagated in the mixing layer. The current approximation of negligible fuel consumption therefore can apply.

Since the effects of reactant consumption are neglected here, Eq. (B9) need not be considered. In addition, the strain rate is considered to be small enough that $Ax\partial T/\partial x$ can be neglected in Eq. (B10). The compressional heating is neglected during cool-flame propagation, and a coordinate system is employed in which the flame is stationary, so that in Eq. (B10) $\partial T/\partial t$ becomes UdT/dx, where U is the propagation velocity, to be determined by upstream heat conduction from the main reaction region where the temperature is near T_{max} of Figure 1. The structure to be sought is one in which the upstream conduction occurs in a convective-diffusive zone, the main reaction occurs in

a reactive-diffusive zone, and a convective-reactive zone is encountered downstream, where the temperature continues to increase but does so more slowly, the temperature always being presumed to be below T_{min} of Figure 1; (the hot flame can develop only when $T > T_{min}$). It will be found that a distinguished convective-reactive-diffusive transition region is needed between the main reaction zone of the cool flame and the convective-reactive region; distinguished zones of this type have been encountered in previous flame-structure analyses, for example in applications of activation-energy asymptotics to ordinary flames with reaction orders greater than unity (Rogg and Williams, 1985).

With the assumptions stated above, Eq. (B10) gives

$$UdT/dx - D_T d^2T/dx^2 = T_Q R_L \tag{23}$$

as the differential equation describing the cool-flame structure, where R_L is given by Eq. (4). Boundary conditions are that $T \to T_o$ as $x \to -\infty$ and that the convective-reactive balance $UdT/dx = (B_L/B_I)\, e^{(b-a)T_H/T}$ develop as $x \to +\infty$. It is necessary that $T_o < T_\beta$ for these cool-frame structures to exist. An asymptotic solution is sought for large values of a Zel'dovich number related to $aT_H(T_{max} - T_o)/T_{max}^2$.

With T_β defined by Eq. (7), the variables

$$\chi = (T - T_o)/(T_\beta - T_o), \quad \xi = xU/D_T \tag{24}$$

are introduced, and the parameters

$$\left.\begin{aligned} &\alpha = (T_\beta - T_o)/T_\beta, \ \beta = T_L(T_\beta - T_o)/T_\beta^2 \\ &\Lambda = [T_Q/(T_\beta - T_o)]\,[(D_T B_L)/(\beta U^2)]\, e^{-T_L/T_\beta} \end{aligned}\right\} \tag{25}$$

are defined, so that Eq. (23) becomes

$$\frac{d\chi}{d\xi} - \frac{d^2\chi}{d\xi^2} = \frac{\beta\Lambda e^{\beta(\chi-1)/[1+\alpha(\chi-1)]}}{1 + e^{(b/a)\beta(\chi-1)/[1+\alpha(\chi-1)]}}, \tag{26}$$

subject to $\chi \to 0$ as $\xi \to -\infty$ and, as $\xi \to +\infty$,

$$d\chi/d\xi \to \beta\Lambda e^{-[(b/a)-1]\beta(\chi-1)/[1+\alpha(\chi-1)]}. \tag{27}$$

Here α measures the temperature increase to the rate maximum (not the increase T_Q associated with heat release), β is a suitable Zel'dovich number, and Λ represents a burning-rate eigenvalue, scaled so that it will be found to be of order unity.

When $1 - \chi$ is positive and of order unity, so that $\beta(1 - \chi) \gg 1$, the reaction rate is exponentially small, and Eq. (26) gives a convective-diffusive balance, the solution to which is $\chi = e^{\xi}$, where the origin of ξ has now been chosen to have $T = T_\beta$ in this outer solution at $x = 0$. Suitable stretched variables for the reactive-diffusive zone are

$$\psi = \beta(\chi - 1), \ \eta = \beta\xi, \tag{28}$$

and in these variables, to leading order Eq. (26) becomes

$$d^2\psi/d\eta^2 = \Lambda e^{\psi}/[1 + e^{(b/a)\psi}], \tag{29}$$

subject to matching conditions, $d\psi/d\eta \to 1$ as $\eta \to -\infty$ and $d\psi/d\eta \to 0$ (but $\psi \to \infty$) as $\eta \to +\infty$. A first integral of this inner problem is readily seen to be

$$(d\psi/d\eta)^2 = 1 - 2\Lambda \int_{-\infty}^{\psi} \{e^{\psi}/[1 + e^{(b/a)\psi}]\}\, d\psi, \tag{30}$$

so that the matching condition for $\eta \to +\infty$ gives

$$\frac{1}{2\Lambda} = \int_{-\infty}^{\infty} \{e^{\psi}/[1 + e^{(b/a)\psi}]\}\, d\psi = I(b/a), \tag{31}$$

where the integral I is given by Eq. (16) (with $c = b/a$). Equation (31) determines the propagation velocity as

$$U = \left\{ \left[\frac{2\pi a/b}{\sin(\pi a/b)} \right] \left[\frac{T_\beta T_Q/T_L}{(T_\beta - T_o)^2} \right] D_T B_L e^{-T_L/T_\beta} \right\}^{1/2}, \tag{32}$$

where use has been made of Eqs. (16) and (25).

Further clarification of the downstream matching that produced this result is desirable. Expansion of Eq. (30) for large ψ shows that, as $\psi \to \infty$,

$$(d\psi/d\eta)^2 \to [2\Lambda/(b/a - 1)] e^{-(b/a - 1)\psi}, \tag{33}$$

which, in view of Eq. (26), suggests that it its appropriate to introduce the transition-zone variable

$$f = \psi - (\ln \beta^2)/(b/a - 1), \tag{34}$$

in terms of which, to leading order in this downstream transition zone, Eq. (26) becomes

$$df/d\xi - d^2f/d\xi^2 = \Lambda e^{-(b/a - 1)f}, \tag{35}$$

free from the expansion parameter β. Equation (35) has a solution that matches to Eq. (33) as $f \to -\infty$ and to Eq. 27 as $f \to +\infty$. Equation (35) thus describes the convective-reactive-diffusive balance in the transition zone to leading order. The full analysis is carried out most easily in the phase plane of f and $df/d\xi$; in fact, there is economy in employing phase planes throughout the analysis, but the relevant equations will not be written here, since in some sense the current presentation is more instructive, in exhibiting more physical content.

Equation (32) has many implications for the propagation of the cool flame. The dependence of the propagation velocity on the rate of low-temperature reaction and on the thermal diffusitivity is the same as that for an ordinary flame. However, the propagation velocity depends inversely on the difference between the crossover temperature T_β and the initial temperature. The propagation velocity approaches infinity as the initial temperature approaches the crossover temperature because the required heating then approaches zero. However, when $T_\beta - T_o$ becomes too small, the expansion parameter β no longer is large, and the quasisteady cool flame ceases to exist, so that the reaction-front propagation becomes transient. For multiple cool flames in chambers with gradually increasing temperatures through compression, each successive flame will propagate faster than its predecessor because of its smaller value of $T_\beta - T_o$.

The higher the activation energy of the reverse step 3b is, compared with the average activation energy of steps 3f and 4, smaller will be the propagation velocity of the cool flame. This conclusion follows from Eq. (5) and the sine factor in Eq. (32) and is caused by the associated decrease in the energy input from the hot boundary of the cool flame by the continuing slow reaction. In general, the cool flame will propagate faster than an ordinary flame having the same reaction rate as the low-temperature reaction and a flame temperature equal to the crossover temperature. This occurs because the required heating, $T_\beta - T_o$, is generally appreciably smaller than the heat relase, T_Q, and because the continuing downstream reaction contributes additional heating that increases U through the sine factor. The conclusion that U may be reasonably large suggests that these cool flames could often occur in practice.

Although each cool flame may propagate at a different velocity because of its different value of $T_\beta - T_o$, the general structure of each is the same. This structure, shown schematically in Figure 5, has a leading convective-diffusive zone followed by a reactive-diffusive zone, as with ordinary flames. In addition, it has a distinguished convective-reactive-diffusive zone downstream from the main reaction zone, which matches to a larger convective-reactive zone downstream. The fact that these flames are found to start with an inert convective-diffusive zone indicates that they resemble ordinary flames more closely that might originally have been expected.

It has been shown (Liñán and Williams, 1995) that after an initial autoignition at one position, ignition fronts propagate away from the point of the autoignition. These ignition fronts are not led by convective-diffusive zones. The cool flame will be generated from the ignition front once the propagation velocity of the front drops below that of the cool flame. Therefore, a high cool-flame velocity favors the development of the cool flame. The peculiarities of the hydrocarbon ignition chemistry can thus lead to a fairly rich variety of ignition phenomena.

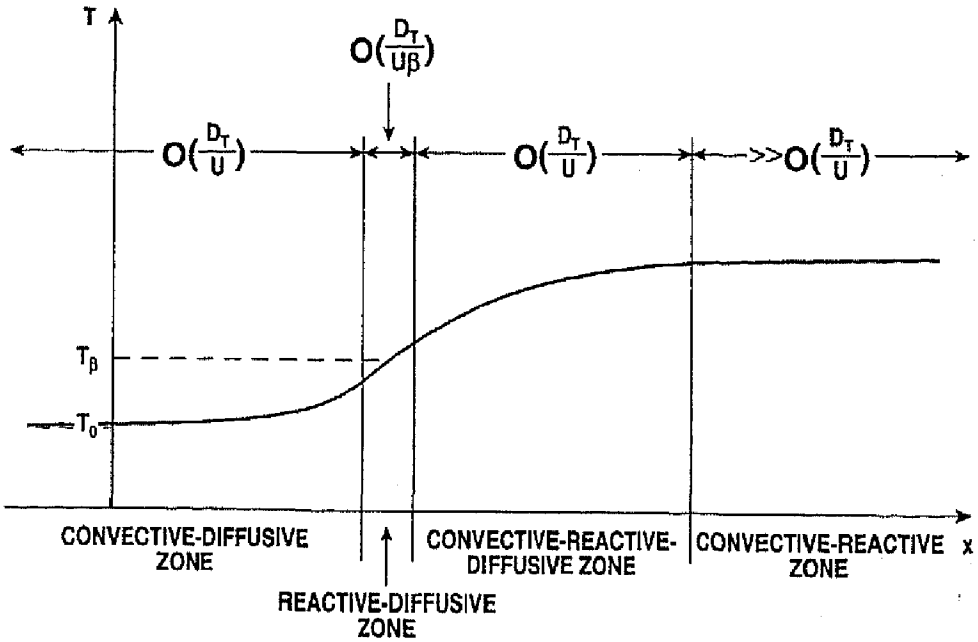

FIGURE 5 A schematic illustration of the cool-flame structure, showing the different distinguished zones.

CONCLUSIONS

The model mechanism for heptane ignition analyzed here does not involve chain branching and therefore needs thermal explosion theory for describing its ignition process. Different chemical-kinetic simplifications arise in different temperature ranges. These ranges can be combined into a high-temperature regime (above roughly 900 K), in which reaction intermediaries maintain steady states and two parallel reactions effectively occur, and a low-temperature regime (below 900 K), in which two sequential reactions occur, the other two steps being negligible. A temperature-explicit approximation provides a useful simplification that encompasses all regimes. Simplified ignition-time formulas have been derived here that enable estimates of adiabatic, isobaric, homogeneous ignition times to be obtained over different temperature ranges, according to different criteria. A variety of different types of temperature-time histories were predicted here for ignition by compressional heating in different regimes. Steadily propagating cool flames were shown to have distinctive structures and propagation velocities and to have reasonable likelihoods of being encountered in compressional ignition of nonhomogeneous hydrocarbon-air mixtures. A formula for the propagation velocities of cool flames was derived. The results provide basic information needed for pursuit of asymptotic analyses of *n*-heptane ignition in nonhomogeneous systems with variable pressure.

In view of the utility of the four-step model on which the present study is based, it would be of interest to try to derive that model systematically through use of reduced chemistry. Although more approximations than usual in reduced chemistry would likely be needed, the results could nevertheless help to clarify which specific elementary rates are most responsible for the success of the four-step description. In addition, it would be of interest to further exploit the temperature-explicit model derived here, to describe alkane ignition processes in nonhomogeneous systems with variable pressure through asymptotic analysis, thereby addressing problems of even more direct relevance to ignition in engines.

Ciezki, H. K. and Adomeit, G. (1993). Shock-Tube Investigation of Self-Ignition of n-Heptane-Air Mixtures Under Engine Relevant Conditions, *Combustion and Flame*, **93**, 421.

Coats, C. M. and Williams, A. (1979). Investigation of Ignition and Combustion of n-Heptane-Oxygen Mixtures. *Seventeenth Symposium (International) on Combustion*, The Combustion Institute, Pittsburgh, pp. 611–621.

Fieweger, K., Blumenthal, R. and Adomeit, G. (1995). Shock-Tube Investigations on the Self-Ignition of Hydrocarbon-Air Mixtures at High pressures. *Twenty-Fifth Symposium (International) on Combustion*, The Combustion Institute, Pittsburgh, pp. 1579–1585.

Lewis, B. and von Elbe, G. (1987). *Combustion, Flames and Explosions of Gases*, 3rd ed., Academic Press, New York, pp. 92–197.
Liñán, A. and Williams, F. A. (1993a). Ignition in an Unsteady Mixing Layer Subject to Strain and Variable Pressure. *Combustion and Flame*, **95**, 31.
Liñán, A. and Williams, F. A. (1993b). *Fundamental Aspects of Combustion*, Oxford University Press, New York.
Liñán, A. and Williams, F. A. (1995). Autoignition of Nonuniform Mixtures in Chambers of Variable Volume. *Combustion Science and Technology*, **105**, 245.
Minetti, R., Carlier, M., Ribaucour, M., Therssen, E. and Sochet, L. R. (1995). A Rapid Compression Machine Investigation of Oxidation and Auto-Ignition of n-Heptane: Measurements and Modeling. *Combustion and Flame*, **102**, 298.
Müller, U. C., Peters, N. and Liñán, A. (1992). Global Kinetics for n-Heptane Ignition at High Pressures. *Twenty-Fourth Symposium (International) on Combustion*, The Combustion Institute, Pittsburgh, pp. 777–784.
Nicoli, C., Clavin, P. and Liñán, A. (1987). Traveling Waves in the Cool Flame Regime. Unpublished.
Rogg, B. and Williams, F. A. (1985). Asymptotic Analysis of Laminar Propagation with Variable Transport Coefficients. *Combustion Science and Technology*, **42**, 301.
Vermeer, D. J., Meyer, J. W. and Oppenheim, A. K. (1972). Auto-Ignition of Hydrocarbons Behind Reflected Shock Waves. *Combustion and Flame*, **18**, 327.
Westbrook, C. K., Warnatz, J. and Pitz, W. J. (1989). A Detailed Chemical Kinetic Reaction Mechanism for the Oxidation of Octane and n-Heptane Over an Extended Temperature Range and Its Application to Analysis of Engine Knock. *Twenty-Second Symposium (International) on Combustion*, The Combustion Institute, Pittsburgh, pp. 893–901.
Williams, F. A. (1985). *Combustion Theory*, 2nd ed., Addison-Wesley Publishing Co., Reading, Mass., p. 580.
Williams, F. W. and Sheinson, R. S. (1973). Manipulation of Cool and Blue Flames in the Winged Vertical Tube Reactor. *Combustion Science and Technology*, **7**, 85.
Williams, K. G., Johnson, J. E. and Carhart, H. W. (1959). The Vertical Tube Reactor-A Tool for Study of Flame Processes. *Seventh Symposium (International) on Combustion*, Butterworths Scientific Publications, London, pp. 392–398.

A. The Four-Step Chemical Model

The chemical model with which the analysis begins is (Müller, Peters and Liñán, 1992)

$$F \rightarrow I, \tag{A1}$$

$$I + 11O \rightarrow P, \tag{A2}$$

$$F + 2O \leftrightarrow J, \tag{A3}$$

$$J + 9O \rightarrow P. \tag{A4}$$

Here F stands for the fuel, nC_7H_{16}, O for the oxidizer, O_2, P for the product combination, $7CO_2 + H_2O$, I for one intermediate combination, taken to be $3C_2H_4 + CH_3 + H$, and J for the other intermediate combination, $OC_7H_{13}O_2H + H_2O$. The first two reactions are most important at higher temperatures, while the third and fourth describe a lower-temperature route. Only the third is reversible, and it has a large activation energy for the reverse step that serves to slow down the low-temperature path at high temperatures.

The rate ω_i of each step i is given by

$$\left.\begin{aligned} \omega_1 &= k_1 n_F, & \omega_2 &= k_2 n_O n_I, \\ \omega_3 &= k_{3f} n_O n_F - k_{3b} n_J, & \omega_4 &= k_4 n_O n_J, \end{aligned}\right\} \tag{A5}$$

where k_i denotes the specific reaction-rate constant for step i (subscripts f and b identifying forward and backward steps 3), and n_j represents the concentration of species j. The first step and the reverse of the third step are unimolecular, while the others are bimolecular.

The Arrhenius forms

$$\left.\begin{aligned} k_1 &= A_1 e^{-T_a/T}, & k_2 &= A_2 e^{-(T_a/3)/T}, \\ k_{3f} &= A_{3f} e^{-T_a/T}, & k_{3b} &= A_{3b} e^{-T_b/T}, \quad k_4 = A_4 e^{-T_c/T}, \end{aligned}\right\} \tag{A6}$$

are employed, where the values of the prefactors are

$$\left.\begin{aligned} &A_1 = 2 \times 10^{10} \mathrm{s}^{-1}, \; A_2 = 2 \times 10^{12} (\mathrm{cm}^3/\mathrm{mol}) \mathrm{s}^{-1}, \\ &A_{3f} = 3 \times 10^{18} (\mathrm{cm}^3/\mathrm{mol}) \mathrm{s}^{-1}, \; A_{3b} = 4 \times 10^{22} \mathrm{s}^{-1}, \; A_4 = 5 \times 10^{13} (\mathrm{cm}^3/\mathrm{mol}) \mathrm{s}^{-1}, \end{aligned}\right\} \tag{A7}$$

and the activation temperatures are

$$T_a = 21{,}650\,\mathrm{K}, \quad T_b = 37{,}285\,\mathrm{K}, \quad T_c = 13{,}230\,\mathrm{K}. \tag{A8}$$

The activation energy for the forward third step is the same as that of the first, while that for the second is one third of these. Ignition times for the temperature and pressure ranges $600\,\mathrm{K} \leqslant T \leqslant 1500\,\mathrm{K}$ and $1\,\mathrm{atm} \leqslant p \leqslant 40\,\mathrm{atm}$, obtained by numerical integrations with these rate parameters, compare quite favorably with those found from numerical integrations with full kinetics and from experiment (Müller, Peters and Liñán, 1992).

The calculations that produced the ignition-time agreement also required thermodynamic data. Isobaric conditions were considered, with a constant average molelcular weight and a constant molar heat capacity at constant pressure of 34.8 J/mol K, representative of the fuel-air mixtures under the conditions of interest. The heat released in each step i was characterized by a temperature rise T_i, defined as the ratio of the enthalpy changes of that step to the molar heat capacity. The values obtained,

$$T_1 = -20{,}400\,\mathrm{K}, \quad T_2 = 149{,}800\,\mathrm{K}, \quad T_3 = 1{,}550\,\mathrm{K}, \quad T_4 = 127{,}850\,\mathrm{K}, \tag{A9}$$

obey the thermodynamically required summation relation

$$T_1 + T_2 = T_3 + T_4 = 129{,}400\,\mathrm{K}. \tag{A10}$$

These same values are employed here.

Characteristic reciprocal times can be defined for each step and plotted as functions of temperature by use of Eqs. (A6), (A7) and (A8). To address ignitions in air, it is best to include the initial oxygen mole fraction X_{O_o} in the definitions of these times, so that the relevant reciprocal times become k_1, $k_2 n X_{O_o}$, $k_{3f} n X_{O_o}$, k_{3b} and $k_4 n X_{O_o}$. Figure 6 shows these times as solid lines for an initially stoichiometric mixture ($X_{F_o} = 0.0187$, $X_{O_o} = 0.2061$) at $p = 40\,\mathrm{atm}$. In Figure 6, the factor n is proportional to pressure p. Relatively small temperature changes are seen in Figure 6 to lead to large changes in

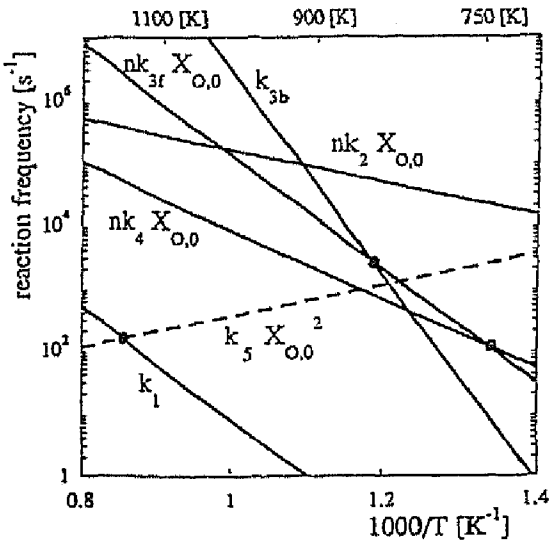

FIGURE 6 An Arrhenius plot of the reciprocal times for different reaction steps for an initially stoichiometric mixture at 40 atm.

ratios of the characteristic times. This produces corresponding changes in ignition regimes with changing temeprature, which can be discussed by investigating isothermal concentration histories at different temperatures (Appendix C).

B. Formulations for Successively Simpler Problems

When specialized to the preceding four-step description, the general equations for species and energy conservation (Liñán and Williams, 1993b) may be written as

$$\rho\left(\frac{\partial X_j}{\partial t}+\boldsymbol{v}\cdot\nabla \mathrm{X}_j\right)=\frac{1}{L_j}\nabla\cdot\left(\frac{\lambda}{c_p}\nabla X_j\right)+w_j,\ j=F,I,J,O,P \tag{B1}$$

and

$$\rho\left(\frac{\partial T}{\partial t}+\boldsymbol{v}\cdot\nabla \mathrm{T}\right)=\nabla\cdot\left(\frac{\lambda}{c_p}\nabla T\right)+\frac{1}{c_p}\frac{dp}{dt}+w_T, \tag{B2}$$

under the assumptions of Appendix A, where ρ is density and $\boldsymbol{v}$ velocity, $X_j=n_j/n$ denotes the mole fraction of species j, L_j its Lewis number (assumed constant) and w_j its molar rate of production times the mean molecular weight $\bar{W}$, and p, λ, and c_p are pressure, thermal conductivity and the specific heat at constant pressure, respectively. The ideal gas equation of state,

$$\rho=p\bar{W}/(R^oT)\equiv\bar{W}n \tag{B3}$$

(with R^o the universal gas constant) is employed. The source terms, under the present approximations, are

$$\left.\begin{aligned} &w_F=\bar{W}(-\omega_1-\omega_3), && w_I=\bar{W}(\omega_1-\omega_2), \quad w_J=\bar{W}(\omega_3-\omega_4),\\ &w_O=\bar{W}(-11\omega_2-2\omega_3-9\omega_4), && w_p=\bar{W}(\omega_2+\omega_4), \end{aligned}\right\} \tag{B4}$$

with ω_i given by Eq. (A5), in which $n_j = X_j n$. In energy conservation, the source term is

$$w_T = \bar{W}(T_1\omega_1 + T_2\omega_2 + T_3\omega_3 + T_4\omega_4). \tag{B5}$$

Mass and momentum conservation complement Eqs. (B1) and (B2). Additional approximations appearing here are the Fick and Fourier laws, the assumption of negligible local radiant energy loss in the differential equation for energy conservation and the assumption of low Mach number, which allows p to be treated solely as a function of t.

Unsteady mixing layers with strain are relevant to ignition in engines (Liñán and Williams, 1993a). For such problems, the mass and tangential-momentum conservation equations can be written as

$$\partial\rho/\partial t + \partial(\rho v)/\partial x + \rho a = 0 \tag{B6}$$

and

$$\rho\left(\frac{\partial a}{\partial t} + v\frac{\partial a}{\partial x} + a^2\right) = \rho_O\left(\frac{da_O}{dt} + a_O^2\right) + Pr\frac{\partial}{\partial x}\left(\frac{\lambda}{c_p}\frac{\partial a}{\partial x}\right), \tag{B7}$$

where x is the coordinate normal to the mixing layer, v the component of the velocity in the x direction, a the strain rate and Pr the Prandtl number (assumed constant). Here the subscript O denotes evaluation of a quantity in the oxidizer stream, and the subscript F will denote evaluation in the fuel stream. The tangential component of velocity is the product of $a(x, t)$ with the tangential distance from the plane of symmetry. The normal component of the equation for conservation of momentum is not written here because it serves only to determine the small variation of pressure in the direction normal to the mixing layer.

In these problems, Eqs. (B1) and (B2) are simplified by neglecting changes in X_j and T in the direction parallel to the mixing layer. Ignition often will occur near the oxidizer stream, where Eq. (B6) can be integrated with respect to x give

$$v = -[a_O + d(\ln\rho_O)/dt]x \equiv -Ax, \tag{B8}$$

in which the origin of the x coordinate has been taken to be the position of zero normal velocity, extrapolated from the velocity profile in the oxidizer stream. If, further, λ/c_p is approximated as constant in the region of interest, then Eqs. (B1) and (B2) become

$$\partial X_j/\partial t - Ax\partial X_j/\partial x - (D_T/L_j)\,\partial^2 X_j/\partial x^2 = W_j, \quad j = F, I, J, O, P \tag{B9}$$

and

$$\partial T/\partial t - Ax\partial T/\partial x - D_T\partial^2 T/\partial x^2 = [(\gamma - 1)/\gamma]\,Td(lnp)\,dt + W_T, \tag{B10}$$

where the thermal diffusivity is

$$D_T = \lambda/(\rho c_p), \tag{B11}$$

the ratio of specific heat is

$$\gamma = c_p/[c_p - (R^o/\bar{W})], \tag{B12}$$

and the source terms are

$$W_F = -k_1 X_F - k_{3f} n X_O X_F + k_{3b} X_J, \tag{B13}$$

$$W_I = k_1 X_F - k_2 n X_O X_I, \tag{B14}$$

$$W_J = k_{3f} n X_O X_F - k_{3b} X_J - k_4 n X_O X_J, \tag{B15}$$

$$W_O = -11 k_2 n X_O X_I - 2 k_{3f} n X_O X_F + 2 k_{3b} X_J - 9 k_4 n X_O X_J, \tag{B16}$$

$$W_P = k_2 n X_O X_I + k_4 n X_O X_J, \tag{B17}$$

$$W_T = T_1 k_1 X_F + T_2 k_2 n X_O X_I + T_3 (k_{3f} n X_O X_F - k_{3b} X_J) + T_4 k_4 n X_O X_J. \tag{B18}$$

Under these approximations, Eqs. (B9) and (B10) can be addressed without further reference to Eqs. (B6) and (B7); the functions $A(t)$ and $p(t)$ are treated as being prescribed in advance.

Initial and boundary conditions are needed to define a well-posed mixing-layer problem. The initial temperature and mole-fraction profiles must be specified,

$$X_j(x, 0) = X_{jo}(x), \quad T(x, 0) = T_o(x). \tag{B19}$$

Normally $X_{Io}(x) = X_{Jo}(x), = X_{Po}(x) = 0$, so that only the functions $X_{Fo}(x)$ and $X_{Oo}(x)$ arise in the initial concentration profiles. The boundary values given in the fuel and oxidizer streams are

$$X_j = X_{jF}(t), \quad T = T_F(t) \tag{B20}$$

and

$$X_j = X_{jO}(t), \quad T = T_O(t), \tag{B21}$$

respectively. Normally $X_{jF}(t) = 0$ for $j \neq F$, $X_{jO}(t) = 0$ for $j \neq O$ and $X_{FF}(t)$, $X_{OO}(t)$, $T_F(t)$ and $T_o(t)$ are specified constants, independent of t.

Further simplifications of this formulation enable a number of different problems to be addressed. One is the problem of the steady, strained mixing layer, obtained by putting $\partial/\partial t = 0$ and $d/dt = 0$ and by deleting the initial conditions of Eq. (B19). Another is the problem of the unsteady, unstrained, constant-pressure mixture layer, obtained by putting $A = 0$ and $dp/dt = 0$. A third is the homogeneous ignition problem with variable pressure, obtained by putting $\partial/\partial x = 0$ and by deleting the boundary conditions in Eqs. (B20) and (B21). The simplest problem is the homogeneous, constant-pressure ignition problem, obtained from the third problem by putting $dp/dt = 0$ as well. This problem is defined by Eqs. (B13) through (B19) with

$$dX_j/dt = W_j, \quad j = F, I, J, O, P, T, \tag{B22}$$

where $X_T \equiv T$.

C. Isothermal Concentration Histories in the Four-Step Model

Different regimes of isothermal chemistry arise in different temperature ranges. It is convenient to address these regimes beginning at the lowest temperature and proceeding to the highest. Although these various regimes under many conditions are not

accurately distinct and are combined to facilitate analysis, it is nevertheless instructive for fixing ideas to exhibit each regime separately.

$T < T_-$

Although Figure 6 shows step 2 to have the highest rate constant at the lowest temperatures, this is irrelevant because step 2 cannot occur until the intermediate I is produced by step 1, and the rate of step 1 is negligible there because k_1 is extremely small. Therefore, only steps and 3 and 4 influence the rate. At the lowest temperature, the rate constant for step 4 is seen in Figure 6 to be high enough that, during a brief initial stage, the intermediate J may be anticipated to rapidly achieve a steady state, yielding from Eq. (B15)

$$X_J = (k_{3f}/k_4)\, X_F, \tag{C1}$$

since step 3b is seen from Figure 6 to be very slow in this regime. Equation (B22) readily gives

$$X_O = X_{Oo} - 11\,(X_{Fo} - X_F) \tag{C2}$$

and

$$dX_F/dt = k_{3f} n X_O X_F \tag{C3}$$

which may easily be integrated. This regime ends when T becomes large enough that the rate of step 4 is no longer large enough compared with the forward rate of step 3 for J to maintain its steady state, at temperature T_- that may be roughly defined by

$$k_{3f}(T_-) = k_4(T_-), \tag{C4}$$

the crossover point of the k_{3f} and k_4 curves in Figure 6, about 750 K. At temperatures above this value, Eq. (C1) is inapplicable, as illustrated, for example, by the observation that it gives $X_J > X_F$.

When temperatures are in the vicinity of T_-, two simultaneous differential equations are needed in describing the isothermal concentration histories, one for X_F and one for X_J. It is then no longer easy to integrate equations for concentration histories exactly, although the qualitative behaviors of the solutions are readily inferred from order-of-magnitude estimates. For quantitative accuracy, if a step is to be considered to be slow, then its rate should be a factor of ten or more below the rate of a step that is considered fast. Extrapolation of the lines in Figure 6 indicates that this order-of-magnitude difference in the characteristic times of steps 3f and 4 does not develop until temperatures are below 650 K. That is Eq. (C4) does not provide a sufficiently conservative estimate of the end of the regime in which the above simplifications apply. Nevertheless, as an idealization that can aid in understanding, crossover conditions are employed in this appendix as boundaries of regimes. With more stringent criteria, some regimes (such as that defined in the following subsection) do not even exist, but their identification can still be instructive concerning the general character of the system.

$T_- < T < T_t$

For temperatures sufficiently above T_-, step 4 is slow enough to allow the concentration of the intermediate J to increase above that of the fuel during a short initial stage in

which step 4 can be neglected and only step 3 is important. This initial stage is followed by a second stage, of longer duration, in which step 4 must be considered as well. So long as the reverse of step 3 is negligible, in the limit of an infinite ratio of the characteristic time of step 4 to that of step 3, fuel would be converted completely to the intermediate J in the initial stage, while J would be converted to product in the second stage. Figure 6 indicates that in fact the reverse of step 3 is not negligibly slow above T_- for $p \leqslant 40$ atm, so that in the initial stage the fuel mole fraction is reduced towards its partial-equilibrium value

$$X_F = X_J k_{3b}/(k_{3f} n X_O), \tag{C5}$$

and the fuel-intermediate pool, with effective mole fraction $X_K = X_F + X_J$, is converted to products in the second stage. The oxygen balance leads to

$$X_O = X_{Oo} + 9(X_K - X_{Fo}) - 2(X_{Fo} - X_F), \tag{C6}$$

which with the approximation given in Eq. (C5) enables the relevant mole fractions to be expressed in terms of X_K. The general differential equation for the second stage under these conditions then becomes

$$dX_K/dt = -k_4 n X_O X_J, \tag{C7}$$

which can be made explicit, if not integrable analytically, by substitutions from above after solving a quadratic. For the conditions of Figure 6, Eq. (C5) shows that near T_- the value of X_F is small compared with X_J, so that $X_K \approx X_J$ and $X_O \approx X_{Oo} + 9X_J - 11X_{Fo}$, and Eq. (C7) is then readily integrated analytically subject to $X_J = X_{Fo}$ at $t = 0$ for the second stage. This solution is no longer valid at a transition temperature T_t defined by crossover of the rate coefficients for the forward and backward rates of step 3,

$$k_{3b}(T_t) = (nX_O)k_{3f}(T_t), \tag{C8}$$

about 850 K in Figure 6. For $T > T_t$ Eq. (C5) indicates that $X_J < X_F$, that is, a steady state for the intermediate J again begins to become valid, now because it is consumed sufficiently rapidly by the reverse of step 3, rather than by step 4.

Figure 6 indicates that the regime just identified will not be well resolved at all under the conditions of the figure for two reasons. First of all, k_{3b} is sufficiently small only near the lowest temperature, and second, k_4 is not really small enough anywhere in this range. The reasonable requirement $k_4 < 10^{-1} k_{3f}$ is not reached until almost 950 K, well above the value of T_t indicated above, and so in fact the first and second stages will not be clearly distinguishable throughout this regime, thereby necessitating the retention of two coupled differential equations simultaneously. The value 950 K is independent of pressure because steps 3f and 4 are both of the same reaction order, but the different order of step 3b leads to a value of T_t that increases with pressure, reaching 950 K at about $p = 400$ atm. Although the rate constants thus indicate that the regime would become resolved at sufficiently high pressures, the validity of the chemical model itself has not been tested at such high pressures, and the model may well fail before the regime can be seen clearly. As the pressure is reduced, the regime narrows, and it disappears entirely ($T_t \to T_-$) at about 4 atm. At extremely low pressures, a new regime

could emerge in which $T_t < T < T_-$, having the same characteristics as that of the previous subsection, except that Eq. (C1) is replaced by $X_J = k_{3f} n X_O X_F / k_{3b}$, and the regime of the previous subsection is then restricted further by $T < T_t < T_-$, but this situation is not worth considering either because the chemical model has not been tested at such low pressures. In general, therefore, the regimes identified in this subsection seem unlikely to ever be clearly identifiable in practice, although the discussion does demonstrate the conceptually interesting phenomenon that, with increasing temperature, in the second stage the intermediate J may go out of steady state then return to steady state, and whille J is out of steady state, the fuel itself achieves steady state, equivalent to partial equilibrium of step 3 (with step 1 totally negligible).

$T_t < T < T_+$

When the steady state applies for the intermediate J as a consequence of the forward and backward stapes 3 being fast, Eq. (C5) give $X_J < X_F$, so that the approximation $X_K = X_F$ may be employed, and Eq. (C7) for the second stage becomes

$$dX_F/dt = -k_4 K_3 n^2 X_O^2 X_F, \tag{C9}$$

where $K_3 = k_{3f}/k_{3b}$ is the equilibrium constant for step 3. Equation (C6) indicates that, in Eq. (C9), Eq. (C2) may again be used as a simplification for X_O. Since Eqs. (A6) and (A8) show that the effective activation temperature in this regime is $T_c + T_a - T_b = -2405\,\mathrm{K}$, a negative value, the reaction rate here decreases with increasing temperature. This is a consequence of the decrease in the steady-state concentration of the intermediate J, which is a reactant in the controlling step 4. The effective rate constant for Eq. (C9) is denoted by

$$k_5 = k_4 K_3 n^2. \tag{C10}$$

The dashed line in Figure 6 shows $k_5 X_{O_0}^2$ in the Arrhenius graph.

As yet, steps 1 and 2 have not played any role in the kinetics because the rate of step 1, the essential initial step for these two processes to occur, has been too small. The decrease in the rate of fuel consumption in the second stage with increasing temperature according to Eq. (C9) eventaully results in the rate of fuel consumption by step 1 becoming comparable with that through steps 3 and 4. Equality of these two rates occurs at the crossover temperature T_+, defined by

$$k_1(T_+) = X_O^2 k_5(T_+) \tag{C11}$$

and seen from Figure 6 to be about 1150 K at 40 atm. If k_1 is independent of p, as Eqs. (A1) and (A5)–(A7) suggest, then this temperature decreases to about 950 K at 4 atm, being relatively strongly pressure dependent, because k_5 is proportional to p^2 according to Eq. (C10); even if the high-temperature initiation step is biomolecular, so that k_1 is proportional to p, then there is still an appreciable decrease in T_+ with decreasing p. Above this temperature, it is no longer permissible to neglect steps 1 and 2. However, T_t also decreases with decreasing p, and all conditions necessary for this regime to exist generally are strongly satisfied (e. g. for temperatures between about 950 K and 1050 K in Fig. 6); the regime is therefore anticipated to be well resolved.

$T > T_+$

For $T > T_+$ there is an initial stage in which the fuel consumption occurs rapidly by step 3. This process produces partial equilibrium of step 3 in the very short time k_{3b}^{-1}, while a second stage begins, in which the dominant fuel consumption occurs through step 1. Since Figure 6 shows that the rate constant for step 2 greatly exceeds that for step 1, this second stage results in the concentration of the intermediate I quickly increasing to its steady-state value,

$$X_I = (k_1/k_2) X_F/(nX_O), \tag{C12}$$

on the time scale $(k_2 n X_{Oo})^{-1}$, intermediate between k_{3b}^{-1} and k_1^{-1}. Subsequently, in a third stage, the intermediates I and J both maintain steady states, and the rate of step 1 dominates both the rate of removal of fuel and the rate of production of products, giving the overall one-step reaction $F + 11O \rightarrow P$, applicable in fact in all of the previous second stages as well (excluding that for $T_- < T < T_i$, for which the reaction is $J + 9O \rightarrow P$). The differential equation for this third stage is simply

$$dX_F/dt = -k_1 X_F, \tag{C13}$$

which is trivially integrable under isothermal conditions. This regime is extremely well resolved for temperatures above about 1200 K at 40 atm and would end only at extremely high temperatures such that Eq. (C12) gives X_I approaching unity.

D. Homogeneous, Isobaric Ignition Times in the Four-Step Model

Although consideration of nonisothermal processes adds another differential equation to the systems just considered, explosion theory may be used to estimate ignition times on the basis of the chemical-kinetic histories discussed above. It is relevant to observe at the outset, from Eqs. (A1)-(A4), that the chemical mechanism can be no more complicated than a straight-chain process and that therefore branched-chain explosions cannot occur in this model. The theory of thermal explosions therefore provides the only candidate for obtaining simple estimates of ignition times. According to this theory, for a one-step, Arrhenius process releasing the amount of energy $c_p \bar{W} T_Q$ per mole of fuel consumed, the ignition time is

$$t_{ign} = T_o^2/(T_Q T_A k_o X_{Fo}), \tag{D1}$$

where T_A is the activation temperature associated with the heat realese, and k_o is the effective first-order specific reaction-rate constant at the initial temperature T_o (Williams, 1985; Liñán and Williams, 1993b). This formula arises by defining the ignition time as the time required for T to increase by an amount T_o^2/T_A and is the first approximation in a formal treatment by activation-energy asymptotics, employing a thermal runaway criterion for ignition. It is of interest to apply Eq. (D1) to each of the four regimes described in Appendix C.

$T_o < T_-$

In this regime, Eqs. (B18) and (B22) readily give

$$dT/dt = (T_3 + T_4) k_{3f} n X_O X_F = -(T_3 + T_4) dX_F/dt, \tag{D2}$$

where Eq. (C3) has been employed in the last equality. For this one-step process, Eqs (A6), (A8), and (A10) imply that $T_Q = 129{,}400\,\mathrm{K}$ and $T_A = 21{,}650\,\mathrm{K}$, and $k_o = k_{3fo} n_o X_{Oo}$ in Eq. (D1). The overall activation energy for t_{ign}^{-1} in this regime is about 45 cal/mole.

This simple reasoning is based on the presumption that ignition occurs in the second stage, rather than in the initial stage of radical buildup-a presumption motivated by observing from Eq. (A9) that the heat release associated with fuel consumption (described by T_3) is negligible compared with that associated with the intermediate consumption (described by T_4). It is necessary, however, to test whether sufficient intermediate consumption may occur during its buildup to cause ignition. For this purpose, the buildup time

$$t_{build} \approx X_J/(k_{3f} n X_O X_F) \approx (k_4 n X_O)_o^{-1} \tag{D3}$$

may be compared with the ignition time obtained above. The criterion $t_{build} \ll t_{ign}$ is then found to be $k_{3f}/k_4 \ll T_o^2/(T_Q T_A X_{Fo})$, which is satisfied only at very low temperatures. At higher temperatures, Eqs. (B18) and (B22) give, approximately,

$$dT/dt = T_4 k_4 n X_O X_J, \tag{D4}$$

since T_3 is negligibly small, and colupled with the approximation

$$dX_J/dt = k_{3f} n X_O X_F, \tag{D5}$$

from Eqs. (B15) and (B22), results in the order-of-magnitude estimate $\Delta T/t_{ign} = T_4 k_4 n X_O (k_{3f} n X_O X_F t_{ign})$, which with $\Delta T = T_0^2/T_A$ produces

$$t_{ign} = T_o (T_4 T_A)^{-1/2} (k_{3fo} k_{4o})^{-1/2} (n_o X_{Oo})^{-1} X_{Fo}^{-1/2}, \tag{D6}$$

in which $T_A = (T_a + T_c)/2 = 17{,}440\,\mathrm{K}$, from Eqs. (A6) and (A8). The consequent lower activation energy, of about 35 kcal/mol, will be more representative of most of this regime. A gradual transition from Eq. (D1) to Eq. (D6) with increasing temperature in this regime may be anticipated, although as an approximation adopted to help illustrate results more clearly, a sharp transition from the higher to the lower activation energy may be presumed to occur when T_o increases through a critical value T_* at which the two ignition times are equal. The value of T_* is then defined by

$$k_{3f}(T_*) = \frac{T_*^2 T_4 (T_a + T_c)}{2 X_{Fo} (T_3 + T_4)^2 T_a^2} k_4(T_*), \tag{D7}$$

which falls within this regime but below 600 K, the low-temperature limit for the validity of the kinetic-model correlation. The low-temperature end of Figure 7 illustrates the ignition-time results thus obtained for $T_o < T_-$.

$T_- < T_o < T_t$

The estimate in Eq. (D6) equally applies in this regime in the vicinity of $T_o = T_-$. In the estimate in Eq. (D3) for the duration of the initial stage, Eq. (C5) must now be employed

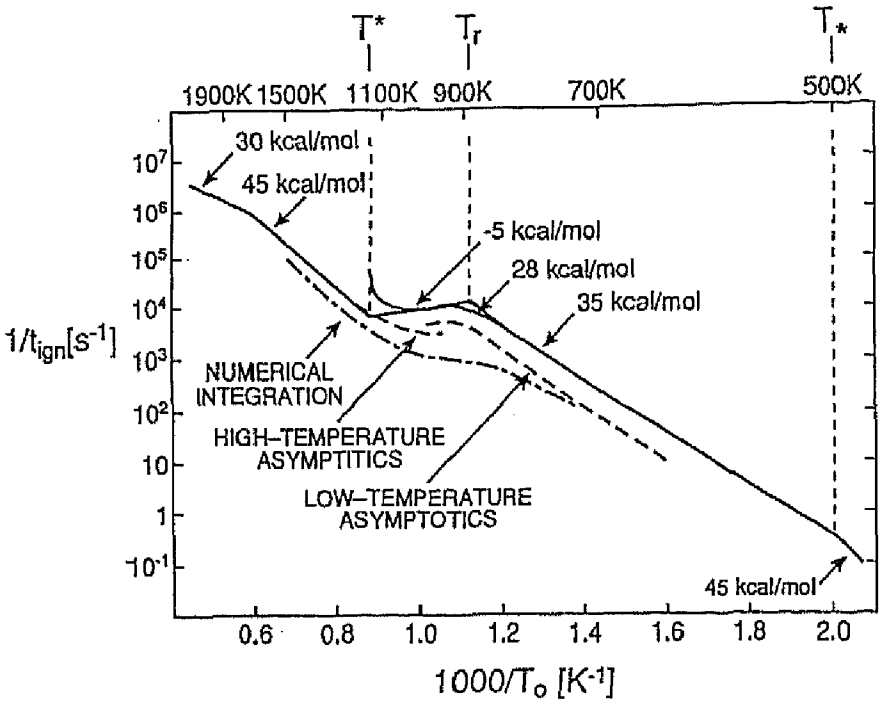

FIGURE 7 A schematic Arrhenius plot of reciprocal ignition times for the conditions of figure 6.

in place of Eq. (C1) in deriving the last equality, and the revised result is $t_{build} \approx k_{3bo}^{-1}$, so that Eq. (D6) holds when it gives $t_{ign} \ll k_{3bo}^{-1}$. Otherwise, the second stage is entered prior to ignition, and Eqs. (B18) and (B22) with T_3 neglected give

$$dT/dt = T_4 k_4 n X_O X_J = -T_4 dX_J/dt, \tag{D8}$$

where Eq. (C7) was used in the second equality; the resulting one-step process conforms with Eq. (D1) with $T_Q = T_4 = 127{,}850$ K, $T_A = T_c = 13{,}230$, and $k_o = k_{4o} n_o X_{Oo}$, yeilding an overall activation energy of about 28 kcal/mol. This last result requires $k_{4o} n_o X_{Oo}/k_{3bo} \ll T_o^2/(T_4 T_c X_{Fo})$ for its validity, which improves with increasing T_o. The activation energy may thus be expected to continue to decrease with increasing temeprature in this regime, although as an approximation Eq. (D6) may be considered to hold below a critical temperature T_s and Eq. (D1) above, where T_s is again defined by equality of the two ignition times,

$$k_4(T_s) = \frac{T_s^2(T_a + T_c)}{2X_{Fo} T_4 T_c^2} k_3(T_s). \tag{D9}$$

Numerically, the resulting T_s typically exceeds T_l, so that this transition is not observed, mainly because the regime itself is too narrow to be distinguished very clearly, as discussed above. In the results shown in Figure 7, a small range of 28 kcal/mol is sketched in for illustrative purposes. However, the main conclusion to be drawn from these considerations is that, for practical purposes, throughout both this and the preceding regime, the thermal runaway occurs during the initial stage, and Eq. (D6) may be used to estimate the ignition time.

$T_i < T_o < T_+$

In this regime, Eqs. (B18) and (B22) with T_3 neglected produce

$$dT/dt = -T_4 dX_F/dt, \tag{D10}$$

with dX_F/dt given by Eq. (C9). The negative activation energy, indicated after Eq. (C9), implies then that a thermal explosion in fact cannot occur in this regime. The reaction rate will decrease with increasing temperatures, until the temperature reaches T_+ and the high-temperature path through steps 1 and 2 begins, exhibiting a positive activation energy. The time required for this to occur may be roughly estimated from Eqs. (C9) and (D10) to be

$$t_{delay} = (T_+ - T_o)/(T_4 X_{Fo} k_{5o} X_{Oo}^2), \tag{D11}$$

where k_5 is defined in Eq. (C6) and shown in Figure 6. This rough estimate is reasonable only when the negative activation energy is not very large. This delay time will provide the major contribution to the ignition time if it is large compared with the ignition time of the regime in which $T > T_+$, as it indeed is, except when T_o approaches T_+ to within about 50 K. Away from this limit, Eq. (D11) gives an activation energy for the ignition time of about -5 kcal/mol. When $T_s > T_i$, there is a critical initial temperature T_r at which t_{delay} of Eq. (D11) equals t_{ign} of Eq. (D6), and above this temperature it will be better to employ Eq. (D11) than Eq. (D6). This temperature, defined by

$$(n_o X_{Oo})^2 k_{3f}(T_r)\, k_4(T_r) = \frac{(T_+ - T_r)^2 (T_a + T_o)}{2 X_{Fo} T_4 T_r^2} k_{3b}^2(T_r), \tag{D12}$$

typically lies near T_i and within the present regime, as illustrated in Figure 7, where the negative activation energy is also indicated, with its bendover sketched towards zero ignition time as T_o approaches T_+, according to Eq. (D11).

Especially in this regime, ignition times may be expected to be strongly dependent on the particular definition that is adopted. For example, a full-chemistry calculation employing a critical radical concentration level to define ignition may give times quite different from those based on attainment of a specified temperature rise, and these, in turn, may differ from times based on eventual thermal runaway. Although the present estimates are geared to thermal runaway, a more detailed runaway analysis is given in the main text.

$T_o > T_+$

In this high-temperature regime, the early stages are nearly energetically neutral according to Eq. (A9), so ignition may be expected to occur after the steady state of Eq. (C12) is established, as may be verified *a posteriori* by comparing the ignition time with relevant times k_{3b}^{-1} and $(nk_2 X_O)^{-1}$, both of which are quite small in this high-temperature regime. Equations (B18), (B22) and (C13) show that

$$dT/dt = -(T_1 + T_2)\, dX_P/dt, \tag{D13}$$

to be used with Eq.(C13). The ignition time is then given by Eq.(D1), with the substitutions $k_o = k_{1o}$, $T_Q = T_1 + T_2$ and $T_A = T_a$. The transition between Eq.(D11) and this result may be estimated to occur at an initial temperature T^* obtained by equating ignition times,

$$k_{3b}(T^*)k_1(T^*) = \frac{(T_+ - T_r)(T_3 + T_4)\,T_a}{T^{*2}T_4}(n_o X_{Oo})\,k_{3f}(T^*)\,k_4(T^*), \qquad \text{(D14)}$$

giving T^* close to T_+. The activation energy for t_{ign} in this regime is about 45 kcal/mol, as illustrated in Figure 7. Figure 6 suggests that at higher temperatures the activation energy will decrease again because nk_2X_O will become too small, but this occurs well above 1500 K, outside the range of the correlation, although its character is also indicated in Figure 7.

The solid straight lines in Figure 7 summarize the reciprocal ignition times obtained here. Improved results can be derived through a formal application of activation-energy asymptotics (Müller, Peters and Liñán, 1992). Efficiencies of the analyses are aided by including more than one of the preceding regimes in a common formulation. Thus, a single low-temperature regime, extending up to a temperature T_o of about 900 K, and a single high-temperature regime, extending down to about 900 K, were considered separately. In the low-temperature regime, steps 1 and 2 are ignored, but steps 3 and 4 are included completely, without any approximation of a steady state for the intermediate J or of partial equilibrium for step 3. In the high-temperature regime, all four steps are included, but steady-state approximations are employed for both intermediates, I and J. As a consequence, there are, in effect, two sequential reactions in the low-temperature regime and two parallel reactions in the high-temperature regime. The changing relative importance of the different steps with changing T_o causes the smooth variations illustrated by the dashed curves in Figure 7. The agreement with results of numerical integrations for the model chemistry are good, except the regime $T_l < T_o < T_+$ (roughly between 800 K and 1100 K), where the predictions are more sensitive to the particular ignition criterion employed. Although the numerical integrations with the four-step model chemistry have not shown a reversal in the intermediate range giving rise to an increase in t_{ign} with increasing T_o, both experiment and numerical integrations with full chemistry do show such a reversal, in qualitative agreement with the present estimates for the four-step model but not with the more rigorous thermal-runaway prediction of the temperature-explicit model in the main text.